Supplemental Material for "Droplet spreading in a wedge: A route to fluid rheology for power-law liquids"

Marcel Moura[a], Vanessa Kern[b], Knut Jørgen Måløy[a,c], Andreas Carlson[b,d], and Eirik G. Flekkøy[a,e]

[a]*PoreLab, the Njord Center, Department of Physics, University of Oslo, NO–0316 Oslo, Norway*
[b]*Department of Mathematics, University of Oslo, NO–0316 Oslo, Norway*
[c]*PoreLab, Department of Geoscience and Petroleum, Norwegian University of Science and Technology, NO–7031 Trondheim, Norway*
[d]*Department of Medical Biochemistry and Biophysics, Umeå University, Sweden*
[e]*Department of Chemistry, Norwegian University of Science and Technology, NO–7491 Trondheim, Norway*

A Experimental Methods

A.1 Preparation of the wedge, polymeric coating and plasma treatment

The key challenge in the preparation of the experiment is ensuring that any types of perturbations to the droplet spreading are minimized. The typical main source of perturbation is contact-line pinning, which may arise from either chemical or mechanical heterogeneities in the solid surface of the plates. To reduce contact-line pinning, we applied a hydrophilic polymeric coating to the inner surfaces of the plates, followed by low-pressure plasma treatment. The coating was created using the two-part PDMS (Polydimethylsiloxane) Dow SYLGARD 184, a silicone elastomer widely used in microfluidics. The PDMS consists of a base and a curing agent, but because it is naturally hydrophobic, we added a third component, a methyl-terminated poly(dimethylsiloxane-b-ethylene oxide) from Polysciences Inc., to act as a hydrophilic agent. We targeted weight ratios of 10 : 1 : 0.2 for the base, curing agent, and hydrophilic agent, respectively, with the hydrophilic agent incorporated while the silicone was still fluid, before curing. The mixture was stirred vigorously for several minutes, then placed in a vacuum chamber to eliminate air bubbles introduced during stirring.

While the coating solution was degassing, we prepared the glass plates by positioning them side by side along their longest edge (76 mm). We connected the plates with a strip of Scotch tape acting as a hinge along the edge (see Fig. 1d). Care was taken to avoid trapping air bubbles, especially along the central edge where the droplet spreading occurs.

Next, we used a Laurell WS-650-23B spin coater to apply the coating solution to the glass slides. We added the degassed PDMS solution to the central part of the plates and spun them at 3000 RPM for 2 minutes, following a brief fast acceleration phase. The spinning was repeated once again to ensure a homogeneous thin layer of the modified PDMS solution. The sample was weighed before and after coating, revealing that approximately 0.09 g of PDMS had been deposited, corresponding to a layer thickness of about 0.05 mm. For reference, the thickness of the Scotch tape beneath the PDMS was estimated at 0.03 mm, and the glass plates themselves were 1.0 mm thick.

After coating, the sample was cured in an oven at 100°C for 1 hour. Once the PDMS was fully cured, we proceeded with the nitrogen plasma treatment. We used a low-pressure plasma system from Diener Electronic for this step. The sample was placed in a sealed plasma chamber, and a vacuum pump reduced the air pressure to 0.15 mbar. A steady nitrogen flow was established to create a nitrogen-rich environment at 0.3 mbar. Plasma was then activated and maintained at 60% power for 3 minutes.

This plasma treatment was crucial for achieving hydrophilicity, as the hydrophilic agent alone was insufficient. PDMS is inherently hydrophobic, with a water-air contact angle around $\Theta = 120^\circ$ [49]. Before plasma treatment, we measured a contact angle of $\Theta = 75^\circ$, using a droplet of xanthan gum solution (2 g/L in water). After plasma treatment, the contact angle decreased to approximately $\Theta = 20^\circ$.

A.2 Preparation of the fluids

The power-law fluids were prepared by mixing different concentrations of xanthan gum in water using a magnetic stirrer. As noted by Whitcomb [50], adding just 1% xanthan gum to water can enhance its viscosity up to 100 000 times at low shear rates, but this increase was limited to only 10 times at high shear rates. We started the procedure by adding 250 g of deionized water in a container that was placed in a magnetic stirrer at a rate high enough to form a visible vortex. The XG was gradually poured onto the side walls of the generated vortex in order to avoid the formation of large clumps. After 1 h, we added 0.25 g of Nigrosin, a strong dark blue water-soluble dye. We also prepared a reference Newtonian fluid by simply mixing glycerol and water, 50% by weight of each part.

After mixing, microscopic air bubbles were inevitably trapped in the fluids, potentially affecting their rheology. To address this, the fluids were placed in a vacuum chamber for degassing.

A.3 Rheological measurements using a commercial rheometer

The rheology of all fluids was characterized using an Anton Paar rheometer model MCR 702e. The results for the effective viscosity μ as a function of the shear rate $\dot{\gamma}$ are shown in Fig. SM1. We conducted tests in which the shear rate $\dot{\gamma}$ was gradually increased from $\dot{\gamma}_{\min} = 0.01\,\mathrm{s}^{-1}$ to $\dot{\gamma}_{\max} = 100\,\mathrm{s}^{-1}$ for XG fluids with concentrations between 1 and 6 g/L; from $\dot{\gamma}_{\min} = 0.1\,\mathrm{s}^{-1}$ to $\dot{\gamma}_{\max} = 100\,\mathrm{s}^{-1}$ for the XG fluid at 0.5 g/L; and from $\dot{\gamma}_{\min} = 1\,\mathrm{s}^{-1}$ to $\dot{\gamma}_{\max} = 100\,\mathrm{s}^{-1}$ for the Newtonian glycerol–water mixture. The higher minimum shear rates used for the two least viscous fluids were necessary because the torque at low shear rates was too small to be reliably measured by the rheometer. Note that all fluids present a power-law regime behavior of the form $\mu \propto \dot{\gamma}^{(n-1)}$ for high values of the shear rate $\dot{\gamma}$ (shown as solid lines in the figure). The fluids became more shear-thinning for higher concentrations of XG, see the concentration and exponent values in the legend. The

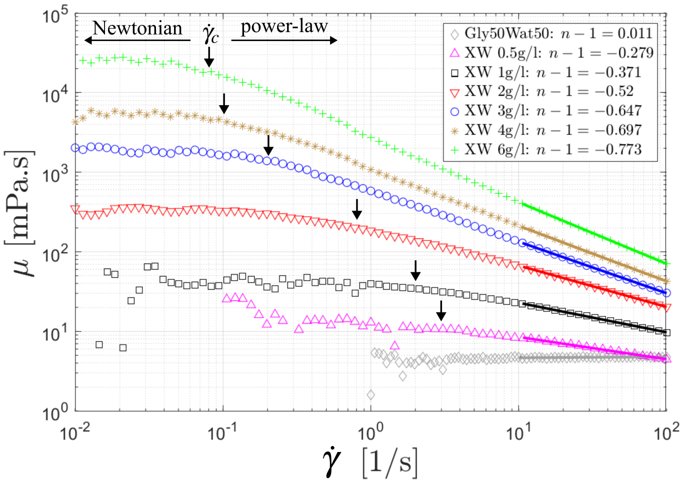

Fig. SM1 Viscosity curve from the Anton Paar MCR 702e rheometer for the different power-law fluids. The reference Newtonian glycerol-water mixture is also shown. The region used to extract the power-law exponent $n-1$ corresponds to the solid lines. The shear rate $\dot{\gamma}_c$, above which the power-lar rheology is observed, is marked by black arrows.

power-law regime is only observed beyond some threshold value $\dot{\gamma}_c$, which depends on the concentration of XG and is indicated by the black arrows. Increasing the XG concentration causes $\dot{\gamma}_c$ to decrease. When $\dot{\gamma} < \dot{\gamma}_c$, the fluids are in a crossover region and for very small shear rates the fluids present a Newtonian behavior with a constant viscosity. Measurements at extremely high shear rates were not performed, however, at such rates, the viscosity of xanthan gum solutions tends to approach that of water[17]. This crossover regime is well documented[13] and was captured in more complex models for the viscosity curve, such as that by Carreau[42].

The μ_0 values that may be read from Fig. SM1 at $\dot{\gamma}_0 = 10\,\mathrm{s}^{-1}$ are roughly within a factor 2 of the values obtained from Eq. (19), using the static contact angle. However, if this value is replaced by a dynamic contact angle Θ_{dyn}, agreement between the values obtained from Fig. SM1 and the prediction of Eq. (19) may be acheived, using $\Theta_{dyn} \approx \pi/3$ as a fitting parameter. This value agrees well with the $\Theta_{dyn} \approx 65^\circ$ obtained by Wijnhorst et al.[40] for Newtonian fluids spreading in an $\alpha = \pi/2$ wedge. This strongly suggests that, while the theoretical exponent n obtained from the measured τ-values is robust in the sense that it does not depend much on the idealizations made in the theory, the prefactor μ_0 does.

In Fig. SM1, we also notice that for the samples presenting the lower values of the effective viscosity, the data begins to fluctuate and becomes unreliable for very low shear rates. We believe this happens because in this zone, the torque imposed by the fluid on the rheometer plates is too small to be reliably measured. This is clearly observed in the curves for XG at $1\,\mathrm{g/L}$, where fluctuations appear below $\dot{\gamma} = 0.04\,\mathrm{s}^{-1}$; for XG at $0.5\,\mathrm{g/L}$, where fluctuations begin below $\dot{\gamma} = 0.3\,\mathrm{s}^{-1}$; and for the Newtonian case, where they start around $\dot{\gamma} = 3\,\mathrm{s}^{-1}$. In this study, we restrict our analysis to the portion of each curve that lies within the power-law regime.

A.4 Droplet placement and effects from films on the plates

A micrometer syringe with a flat-tipped needle is used to deposit a droplet of the specified liquid at the wedge's center. The external diameter of the needle is $1.80\,\mathrm{mm}$ and the droplet volume (set on the syringe) is approximately $20\,\mu\mathrm{L}$. The micrometric needle is positioned in an arm connected to a translation stage which allowed for x, y and z translation to position the droplet in the wedge. The procedure of placing one droplet consisted in first generating the pendant droplet on the needle and then slowly moving the translation stage down until the droplet touched the inner sides of the plates. It would then disconnect from the needle and start spreading sideways, see Fig. 1. Notice that once the droplet touches the glass plates, it creates a wetted region close to the center, which persists as the experiment progresses. This can be seen on Fig. 1c) as the darker patch just below the tip of the needle in the central part of the image. The presence of this film can cause the droplet shape for small x values (close to the center) to deviate from the theoretically predicted shapes, where this artifact was not present. The lateral extent of this region is of the order of $0.3\,\mathrm{cm}$ in both directions, so in our analysis we have ignored the initial frames of the dynamics, in which the droplet spreading may be more affected by these films.

A.5 Experiments with highly wetting silicone oils using a simpler wedge construction

For highly wetting liquids, such as silicone oils, contact-line pinning is naturally reduced, and a simpler setup with only the glass wedge without any polymeric coating or plasma treatment is sufficient. As a first step in the development of our technique, we performed experiments with this simpler wedge construction using silicone oils with kinematic viscosities $50\,\mathrm{cSt}$, $100\,\mathrm{cSt}$, and $350\,\mathrm{cSt}$. In Fig. SM2a) we show snapshots of the experiment with the 100 cSt silicone oil. The transparent silicon oil appears red because of a convenient lensing effect: A red tape is positioned behind the wedge and the contrast in refracting indices causes the droplet to refract the red light into the camera, thus avoiding the need for dyes. The interval between the first and last snapshots was $\Delta t = 10\,\mathrm{s}$. The spreading dynamics is seen in Fig. SM2b) where we see that all exponents show values $\tau = 0.43 \pm 0.03$, obtained from the black guide-to-the-eye line. These findings are consistent with the fact that silicone oil is a Newtonian fluid with a theoretical value $\tau = 0.4$, which results from setting $n = 1$ in Eq. (14). In this experiment, the wedge had an opening angle of $\alpha = 20^\circ$, and the droplet was positioned by hand instead of employing the more precise arrangement with a micrometric syringe. Images were recorded with a DSLR camera in video mode. Notice that, even though the fluids are significantly different, with viscosities varying by a factor of 7, the exponent is rather stable. The specific value of the viscosity, as well as the opening angle α, enters in the prefactor governing the scaling through the 'diffusion coefficient' D_0 in Eq. (9) but do not affect the exponent τ.

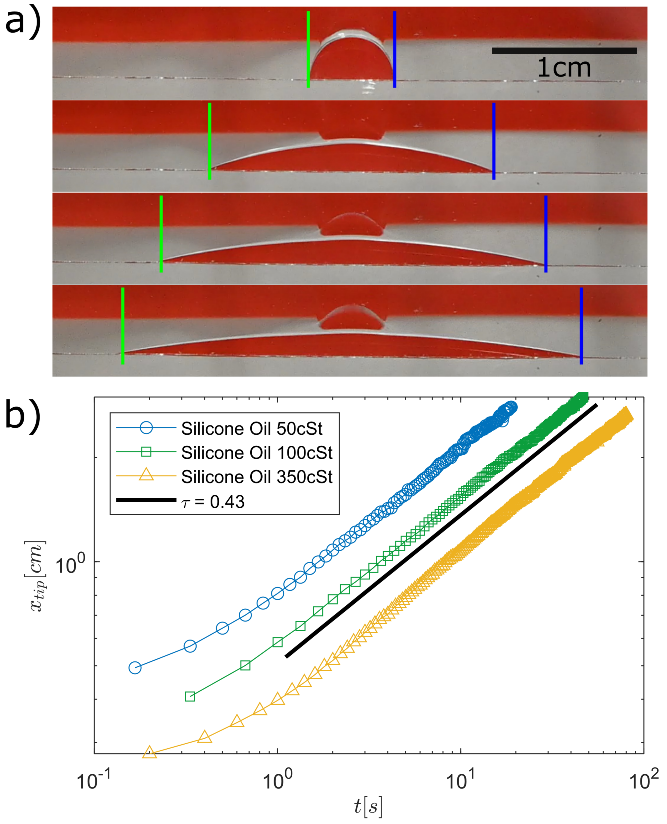

Fig. SM2 a) Snapshots showing the evolution of a droplet of highly wetting silicone oil with a viscosity 100 cSt in the wedge composed only of two glass slides. The interval between the top and bottom snapshots is $\Delta t = 10\,\mathrm{s}$. b) The spreading dynamics of three silicone oils with viscosities $50\,\mathrm{cSt}$, $100\,\mathrm{cSt}$, and $350\,\mathrm{cSt}$ show similar exponents $\tau = 0.43 \pm 0.03$, (black line), consistent with the theoretical value $\tau = 0.4$ predicted for a Newtonian fluid. The data is shifted horizontally by different values to aid visualization.

A.6 Estimation of cross-sectional area of droplet from experimental height profile

In the experiments the cross-sectional area $A(x,t)$ is affected by the curvature of the edge as shown schematically in Fig. 1d). If we ignore this effect, the computed volume of the droplet differs from the known value V_0, which is injected by the needle. The effective height h measured experimentally is the vertical distance from the top of the liquid-air interface and the curved segment in Fig. 1d), which itself is at a distance $\approx h_0$ from the extrapolated, sharp edge of the wedge. We can then estimate $A(x,t)$ as the difference between the area of the triangular wedge (ideal case with sharp corner) and the void space under the curved segment seen in Fig. 1d). From a simple geometrical argument we get

$$A \approx (h+h_0)^2 \tan\left(\frac{\alpha}{2}\right) - h_0^2 \tan\left(\frac{\alpha}{2}\right) = (h^2 + 2hh_0)\tan\left(\frac{\alpha}{2}\right). \quad \text{(SM1)}$$

The vertically projected effective height h is what is shown in Fig. 3a). Notice that this is slightly different from h seen in Fig. 1 but can be obtained from the latter as $h\cos(\alpha/2) - h_0$.

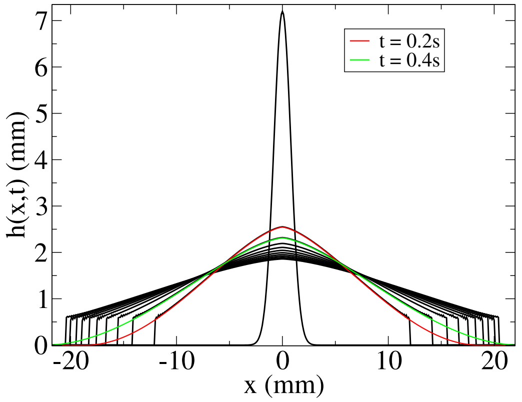

Fig. SM3 The film height as a function of position along the corner at different times when the rheological exponent $n = 0.48$. The black lines derive from the numerical solutions of Eq. (8) using $h(x,t) = \sqrt{2A(x,t)/\alpha}$, while the colored lines show the corresponding analytical solution of Eq. (10) and Eq. (17) for two different times. The taller central curve shows the initial profile of the droplet. A volume of $19\,\mathrm{mm}^3$, initial half-width $w_0 = 0.8\,\mathrm{mm}$, and corner radius of $h_0 = 0.6\,\mathrm{mm}$ were used as parameters for all curves.

B Numerical model

In Fig. SM3 the droplet height $h(x,t) = \sqrt{2A(x,t)/\alpha}$ is plotted as a function of position, where we have taken the normalization to be $\int dx A(x,t) = 19\,\mathrm{mm}^3$, approximating the experimental value. Note that the analytic solution (red and green curves for times given in the legend) has a cusp at $x = 0$ where the second spatial derivative of $h(x,t)$ diverges, while the numerical solution is initialized with the smooth Gaussian $\propto \exp(-x^2/w_0^2)$ (shown as the taller curve). Nevertheless, the numerical solution converges to the analytical solution (red curve) with the same droplet volume within 1‰ during the first 1/10 of the time span, except at the cut-off point $h \approx h_0$, where a weak numerical oscillation around the analytic solutions causes deviations of the order 1%. This shows that the numerical solution quickly converges to the analytical shape prediction, except for the values where h is below the h_0-cutoff. Figure SM4 shows that $x_{tip}(t)$, when $h_0 = 0.6\,\mathrm{mm}$ and $w = 0.8\,\mathrm{mm}$, is well approximated by a power law, that is, that it yields straight lines on a log-log plot. In Fig. SM5 the slopes of these plots are given, showing the variation of τ_c with the corner curvature h_0. Note that they extrapolate well to the analytic value given by the red dot. The deviation from the theoretical τ value decreases with decreasing h_0, as expected.

C Replacement of Darcy's law for a power-law fluid

We need the relationship between the pressure gradient and the average flow velocity of a power-law fluid, where the viscous stress scales as $\dot{\gamma}^n$, where $\dot{\gamma}$ is the shear rate, and n is the rheological exponent, which for a shear-thinning fluid is smaller than unity. When $n = 1$ the fluid is Newtonian. Just as the viscous stress in a Newtonian fluid, the non-Newtonian fluid stress tensor can only depend on the symmetric part of the velocity gradient. For an incompressible fluid the total stress tensor, which includes

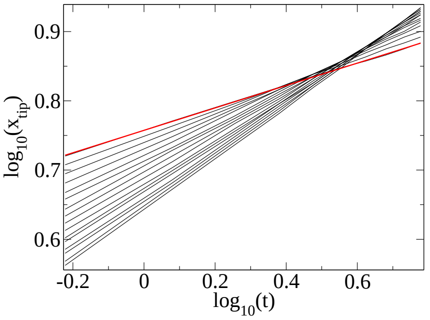

Fig. SM4 The position of the right droplet tip as a function of time for n-values in the range $0.25-1.0$ (black curves). The red curve is a linear fit to the black $n=0.25$ curve, which it nearly covers. All other parameters are as in Fig. SM3.

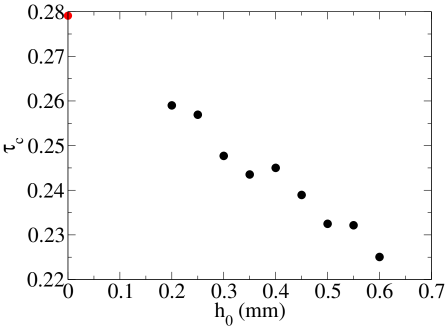

Fig. SM5 The measured slopes τ_c derived from the numerical solution of Eq. (8) versus the radius of curvature of the corner h_0. Here $n=0.48$ and the red dot shows the theoretical value given in Eq. (14).

the pressure P, may be cast in the covariant form,

$$\sigma_{tot\,ij} = -\delta_{ij}P + \eta_0\dot{\gamma}_{ij}(\dot{\gamma}_{kl}\dot{\gamma}_{kl})^{(n-1)/2}\,, \tag{SM2}$$

where P is the pressure, δ_{ij} the Kronecker delta function, and summation over repeated indices is implied. The viscosity coefficient (in units of Pas^n) may be decomposed into $\eta_0 = \mu_0\dot{\gamma}_0^{1-n}$, where μ_0 (in units of Pa s) is the viscosity at the shear rate $\dot{\gamma}_0$. The strain rate tensor is given by

$$\dot{\gamma}_{ij} = \frac{\partial u_i}{\partial x_j} + \frac{\partial u_j}{\partial x_i}\,, \tag{SM3}$$

and the stress balance equation reads

$$\nabla\cdot\sigma_{tot} = 0\,. \tag{SM4}$$

When $n=1$, this equation reduces to the Stokes equation.

Introducing a characteristic length h, which could be the channel width, this equation may be written in terms of the non-dimensional primed quantities defined through

$$\begin{aligned} x_i &= hx_i' \\ u_i &= \dot{\gamma}_0 hu_i' \\ \dot{\gamma}_{ij} &= \dot{\gamma}_0\dot{\gamma}_{ij}' \\ \nabla &= \frac{1}{h}\nabla'\,. \end{aligned} \tag{SM5}$$

Writing the pressure gradient as

$$\nabla P = -|\partial P/\partial x|\mathbf{e}\,, \tag{SM6}$$

where $\mathbf{e}$ is the unit vector in the opposite direction of the pressure gradient, Eq. (SM4) may be written as

$$\mathbf{e} = -\nabla'\cdot\left(\dot{\tilde{\gamma}}\left(\dot{\tilde{\gamma}}^2\right)^{(n-1)/2}\right)\,, \tag{SM7}$$

where $\tilde{\gamma} = \gamma'/G^{1/n}$ and we have introduced the dimensionless ratio between pressure forces and viscous forces, and

$$G = \frac{|\partial P/\partial x|h}{\mu_0\dot{\gamma}_0} \tag{SM8}$$

which is thus a non-dimensionalized pressure gradient. Since the boundary conditions may be given in terms of $\mathbf{u}'(\mathbf{x}_B')$ where $\mathbf{x}_B$ are boundary coordinates, the stress balance equation yields a solution of the form

$$\tilde{\gamma}_{ij} = f_{ij}(\mathbf{x}')\,, \tag{SM9}$$

which in turn gives

$$\dot{\gamma}_{ij}' = f_{ij}(\mathbf{x}')G^{1/n} \sim \frac{\partial u_i'}{\partial x_j'}\,. \tag{SM10}$$

Integrating this equation for the velocity component along the wedge gives

$$u' = G^{1/n}F_n(\mathbf{x}')\,, \tag{SM11}$$

for some other dimensionless function F_n, which in turn gives

$$u = G^{1/n}\dot{\gamma}_0 hF_n(\mathbf{x}')\,. \tag{SM12}$$

Averaging over a cross section of the flow gives

$$\bar{u} = G^{1/n}\dot{\gamma}_0 hQ_n = \left(\frac{|\partial P/\partial x|}{\eta_0}\right)^{1/n} h^{1+1/n}Q_n\,. \tag{SM13}$$

It is possible to calculate Q_n in the lubrication approximation, assuming that the flow is governed by the gradients of u in the angular direction (normal to the wedge walls) alone.

We shall start with the velocity field $u(x)$ in the z-direction in a straight channel of half-width a and a coordinate x in the direction transverse to the flow where $x=0$ in the middle. The velocity satisfies the boundary condition $u(\pm a)=0$. Then, Eq. (SM4) reduces to

$$2^{\frac{1-n}{2}}\frac{|\partial P/\partial x|}{\eta_0} - \partial_x((-\partial_x u)^n) = 0 \tag{SM14}$$

for $x > 0$. This equation is easily integrated to yield

$$u(x) = 2^{\frac{1-n}{2n}} \frac{n}{n+1} \left(\frac{|\partial P/\partial x|}{\eta_0} \right)^{1/n} (a^{\frac{n+1}{n}} - x^{\frac{n+1}{n}}) , \tag{SM15}$$

which has the cross-sectional average,

$$\overline{u} = \frac{1}{a} \int_0^a dx u(x) = 2^{\frac{1-n}{2n}} \frac{n}{2n+1} \left(\frac{|\partial P/\partial x|}{\eta_0} \right)^{1/n} a^{\frac{n+1}{n}} . \tag{SM16}$$

This expression agrees with Darcy's law in a channel of half-width h in the Newtonian $n = 1$ case where $\overline{u} = h^2 |\partial P/\partial x|/(3\eta_0)$.

Now, we return to the wedge geometry. Neglecting the effects of transverse flow on the pressure, the pressure gradient points in the x-direction and is constant over any fixed x plane inside the fluid. For a narrow wedge we may therefore approximate the flow as a superposition of channel flows with half-widths $\alpha r/2$. This approximation is limited to small α- values as it assumes that the velocity variations are dominantly in the angular direction and negligible in the radial direction. So, we replace $a \to \alpha r/2$, thereby obtaining a lubrication approximation $\overline{u}(r)$ to the flow at a distance r to the corner. Averaging $\overline{u}(r)$ over the cross-sectional area

$$\langle u \rangle = \frac{2}{h^2} \int_0^h dr r \overline{u}(r) \tag{SM17}$$

yields the volume flux

$$q = \frac{\alpha h^2}{2} \langle u \rangle = Q_n \left(\frac{|\partial P/\partial x|}{\eta_0} \right)^{1/n} h^{3+1/n} , \tag{SM18}$$

where

$$Q_n = \frac{2^{\frac{1+n}{2n}} n^2}{(2n+1)(3n+1)} \left(\frac{\alpha}{2} \right)^{\frac{2n+1}{n}} , \tag{SM19}$$

which is the desired result.